

Phonon properties of copper oxide phases from first principles

Marcel Giar,^{*} Markus Heinemann, and Christian Heiliger[†]

*Institut für Theoretische Physik, Justus-Liebig-Universität Gießen, Heinrich-Buff-Ring 16, 35392 Gießen, Germany
and Zentrum für Materialforschung, Justus-Liebig-Universität Gießen, Heinrich-Buff-Ring 16, 35392 Gießen, Germany*

(Received 3 February 2017; revised manuscript received 22 June 2017; published 3 August 2017)

We present density functional theory (DFT) calculations on phonon dispersions, phonon density of states, and thermodynamic quantities for the three copper oxide phases Cu_2O , Cu_4O_3 , and CuO . For monoclinic CuO we consider the correct antiferromagnetic ground state. Sound velocities for the acoustic phonon branches and Debye temperatures are calculated and are found to be in good agreement with experiment. We further show how the method for the treatment of dipole-dipole interactions in dynamical matrices of Gonze and Lee [*Phys. Rev. B* **55**, 10355 (1997)] may be incorporated in the real-space (direct) method for interatomic force constants (FCs). The role of the long-ranged dipole-dipole interactions in the phonon dispersion is discussed. Based on this method, we outline a perturbationlike scheme to compute first-order derivatives of the phonon mode frequencies with respect to the wave vector which can be used to compute velocities of sound.

DOI: [10.1103/PhysRevB.96.075202](https://doi.org/10.1103/PhysRevB.96.075202)

I. INTRODUCTION

Copper oxides are known to exist in three modifications: cubic Cu_2O (cuprite), monoclinic CuO (tenorite), and tetragonal Cu_4O_3 (paramelaconite). Among these, the naturally p -type [1–3] conducting cuprite has regained particular attention for solar cell applications and consequently has become well-studied, experimentally [4–13] and theoretically [13–26], over the last decades. The monoclinic tenorite phase has been considered for solar cell applications [10], and high- T_C superconductors [27]. In recent years, density functional theory (DFT) based investigations within the framework of LDA + U [26,28], hybrid functionals [26,29], and many-body perturbation theory [13,30] concentrated on the electronic structure which is governed by the interaction of the O $2p$ and Cu $3d$ states [28,30]. Experimental investigations have succeeded in understanding the magnetic and related structural properties [31–38]. It was found that there exist two antiferromagnetic (AFM) orderings [32,34] with differing Néel temperatures $T_N^{(1)} = 231$ K (incommensurable phase), and $T_N^{(2)} = 213$ K (commensurable phase) [32–36]. In the low-temperature ($T < T_N^{(2)}$) AFM phase with eight formula units per magnetic unit cell, apart from the Cu^{2+} ions (magnetic moment of $\sim 0.65\mu_B$), the oxygen ions also carry nonzero magnetic moments of $\sim 0.14\mu_B$ [32]. Tetragonal, antiferromagnetically ordered paramelaconite is a phase considered to be intermediate to cuprite and tenorite as it contains Cu atoms in two oxidation states, $\text{Cu}^+[\text{Cu(I)}]$ and $\text{Cu}^{2+}[\text{Cu(II)}]$ [39]. In recent years, efforts have been made to explore the electronic properties experimentally as well as computationally [10,13,26,40–42].

As far as lattice dynamics are concerned, experimental studies of the past decades involving for example inelastic neutron scattering, Raman spectroscopy, and IR measurements, in particular focused on the cubic cuprite [43–67] and the monoclinic tenorite [10,38,68–86] phase. For the latter, in the

low temperature regime ($T < T_N^{(2)}$) modes additional to those expected from a factor group analysis of the C_{2h}^6 space group have been observed [38,69,72,74,82]. This was taken as the lattice dynamical indication for the formation of a magnetic superlattice below the Néel temperature [82]. For some modes, in addition, a strong dependence on temperature below $T_N^{(2)}$ was found which finally was attributed to a strong coupling of the corresponding phonon modes to the magnetic ordering, sometimes termed spin-phonon coupling [82]. Only recently, Raman spectra of the intermediate paramelaconite phase of Cu_4O_3 have been reported for samples grown by magnetron sputtering [10,85].

DFT-based approaches to vibrational properties of solids within the harmonic approximation nowadays either rely on the supercell real-space (direct method) [87–89] or density functional perturbation theory (DFPT, see, e.g., Refs. [90–93]). Within the direct method, interatomic force constants (FCs) are calculated using Hellman-Feynman forces resulting from displacements of single atoms from their equilibrium positions. In the linear response method employed within the framework of DFPT, dynamical matrices are computed in reciprocal space on a grid of wave vectors from first-order derivatives of the wave functions with respect to atomic displacements. Both approaches essentially yield the same information, however, they differ in complexity and practicability.

To date, calculations on vibrational properties of copper oxide phases have been rather rare. While the early studies relied on rigid ion models [44,48], more recent investigations employed *ab initio* methods in order to describe the phononic structure within the harmonic approximation [42,66,85,86,94,95]. Calculations involving Cu_2O have made use of the direct method as well as DFPT [66,94,95]. For the tenorite and paramelaconite phases, recent calculations are solely based on the direct method [42,85,86]. However, apart from the case of Cu_2O [66,95] the polar nature of the chemical bonding has not been considered in the calculations of the phonon properties of copper oxide phases. In polar insulating crystals the FCs are long ranged in real space due to the creation of dipoles through atomic displacements. This requires us to consider separately a short-ranged and a Coulomb part of the dynamical matrices [92,93]. Furthermore, in the case of

^{*}marcel.giar@theo.physik.uni-giessen.de

[†]christian.heiliger@physik.uni-giessen.de

monoclinic CuO, the correct ground state magnetic order [32] has not been investigated yet [85,86].

In view of this, we shall show in this work how long-ranged dipole-dipole interactions can be treated in dynamical matrices obtained from the direct method following the method of Gonze and Lee [92], which is conventionally used in conjunction with dynamical matrices from DFPT calculations. The emerging effect on phonon dispersion relations will be discussed. Apart from that, based on the method of Gonze and Lee [92], we outline a scheme that allows us to calculate first-order derivatives of the phonon mode frequencies with respect to the wave vector. This scheme is used to obtain velocities of sound along selected directions. As a matter of fact, the AFM ground state for CuO [32] ($T < T_N^{(2)}$) is considered in all calculations presented for this phase.

II. METHODS

A. The method of Gonze and Lee for the treatment of dipole-dipole interactions in dynamical matrices

For insulating materials with polar bonds (as in the case of copper oxides) dynamical matrices exhibit a contribution through dipole-dipole interactions leading to a separation of the form [92]

$$\tilde{C}_{\kappa'\nu}^{\kappa\mu}(\mathbf{q}) = \text{sr}\tilde{C}_{\kappa'\nu}^{\kappa\mu}(\mathbf{q}) + \text{dd}\tilde{C}_{\kappa'\nu}^{\kappa\mu}(\mathbf{q}), \quad (1)$$

where the contributions to this ‘‘full’’ dynamical matrix are a short-ranged (sr; non-Coulomb) and a dipole-dipole (dd; Coulomb) part, and κ, κ' label atoms in the unit cell while μ, ν are cartesian directions.

Independently of Eq. (1), full dynamical matrices at wave vector \mathbf{q} within the first Brillouin zone (BZ) are given through a lattice Fourier transform of the interatomic force constants (FCs) $C_{l'\kappa'\nu}^{l\kappa\mu}$:

$$\tilde{C}_{\kappa'\nu}^{\kappa\mu}(\mathbf{q}) = \sum_{l'} C_{l'\kappa'\nu}^{l\kappa\mu} e^{+i\mathbf{q}^T(\mathbf{R}_{l'} - \mathbf{R}_\nu)}, \quad (2)$$

where l, l' refer to unit cells within the crystal, and due to translational invariance it holds that $C_{l'\kappa'\nu}^{l\kappa\mu} = C_{l'-l\kappa'\nu}^{0\kappa\mu}$. The sum of Eq. (2) converges slowly for polar insulators since the FCs in real space (more specifically the dipole-dipole part) only decrease as the inverse of the third power of the interatomic distance $\mathbf{d}_{l'\kappa'}^{0\kappa} = \mathbf{R}_{l'} + \mathbf{x}_{\kappa'} - \mathbf{x}_\kappa$ [92,96], where \mathbf{x}_κ denotes an atomic position vector in the unit cell. Mind that for the FCs a similar decomposition into a short- and a long-ranged part holds as for the full dynamical matrices, and the short-ranged part is expected to decay (at least) as the inverse of the fourth power of the interatomic distance [92]. As a result, the sum in Eq. (2) is rapidly convergent when the short-ranged FCs instead of the full (short-ranged+dipole-dipole: $C_{l'\kappa'\nu}^{0\kappa\mu}$) FCs are to be Fourier transformed.

Indeed, this is the fact to be exploited in order to bypass the issue of slow convergence of the Fourier sum. Gonze and Lee [92] suggested to use the partitioning of the full dynamical matrix [according to Eq. (1)], and to calculate instead of Eq. (2):

$$\tilde{C}_{\kappa'\nu}^{\kappa\mu}(\mathbf{q}) = \sum_{l'} \text{sr}C_{l'\kappa'\nu}^{0\kappa\mu} e^{+i\mathbf{q}^T\mathbf{R}_{l'}} + \text{dd}\tilde{C}_{\kappa'\nu}^{\kappa\mu}(\mathbf{q}), \quad (3)$$

i.e., compute the Fourier transform only for the short-ranged FCs and treat the dipole-dipole part separately.

The method due to Gonze and Lee [92] has traditionally been used in the framework of DFPT [97,98], and proceeds along the following lines: Using the linear response approach (i.e., DFPT) full dynamical matrices are directly computed on a predefined grid of $N_{\mathbf{q}}$ wave vectors ($\mathcal{G} = \{\mathbf{q}_i\}_{i=1,\dots,N_{\mathbf{q}}}$) that homogeneously samples the BZ [90,92,93]. Starting from these full dynamical matrices $\{\tilde{C}_{\kappa'\nu}^{\kappa\mu}(\mathbf{q}_i)\}_{i=1,\dots,N_{\mathbf{q}}}$, the short-ranged part is isolated by subtracting the dipole-dipole part $\forall \mathbf{q}_i \in \mathcal{G}$:

$$\text{sr}\tilde{C}_{\kappa'\nu}^{\kappa\mu}(\mathbf{q}_i) = \tilde{C}_{\kappa'\nu}^{\kappa\mu}(\mathbf{q}_i) - \text{dd}\tilde{C}_{\kappa'\nu}^{\kappa\mu}(\mathbf{q}_i). \quad (4)$$

The dipole-dipole part can be dealt with using Ewald summation techniques (Λ : Ewald parameter) [92]. This summation is split into sums over reciprocal space and real space lattice vectors (\mathbf{G} and \mathbf{R}_l), and a limiting contribution. For a convenient choice of Λ the sums in reciprocal and real space are carried out until convergence. With the low-frequency dielectric permittivity $\epsilon_{\mu\nu}^\infty$, and the Born effective charges $Z_{\kappa,\mu\nu}^*$, the expression for $\text{dd}\tilde{C}_{\kappa'\nu}^{\kappa\mu}(\mathbf{q})$ can be computed from the following set of equations for arbitrary \mathbf{q} in the BZ [92]:

$$\begin{aligned} \text{dd}\tilde{C}_{\kappa'\nu}^{\kappa\mu}(\mathbf{q}) &= \frac{4\pi}{\Omega_0} \sum_{\substack{\mathbf{K} \neq 0 \\ \mathbf{G} \text{ with} \\ \mathbf{K} = \mathbf{q} + \mathbf{G}}} K_\mu K_\nu F_0(\mathbf{K}) e^{i\mathbf{K}^T(\mathbf{x}_\kappa - \mathbf{x}_{\kappa'})} \\ &\quad - \sum_{l, D \neq 0} \Lambda^3 H_{\mu\nu}(\Lambda \Delta, \Lambda D) \frac{e^{i\mathbf{q}^T \mathbf{R}_l}}{\sqrt{\det \epsilon^\infty}} \\ &\quad - \frac{4}{3\sqrt{\pi}} \frac{\Lambda^3}{\sqrt{\det \epsilon^\infty}} \delta_{\kappa\kappa'} (\epsilon^\infty)_{\mu\nu}^{-1}, \end{aligned} \quad (5a)$$

$$\begin{aligned} \text{dd}\tilde{C}_{\kappa'\nu}^{\kappa\mu}(\mathbf{q}) &= \sum_{\mu'\nu'} Z_{\kappa,\mu'\mu}^* Z_{\kappa',\nu'\nu}^* \text{dd}\tilde{C}_{\kappa'\nu'}^{\kappa\mu'}(\mathbf{q}) \\ &\quad - \delta_{\kappa\kappa'} \sum_{\kappa'', \mu''\nu''} Z_{\kappa,\mu''\mu}^* Z_{\kappa'',\nu''\nu}^* \text{dd}\tilde{C}_{\kappa''\nu''}^{\kappa\mu'}(\mathbf{q} = \mathbf{0}). \end{aligned} \quad (5b)$$

We use the abbreviations $\Delta_\mu \equiv \Delta_{l'\kappa',\mu}^{0\kappa} = \sum_\nu (\epsilon^\infty)_{\mu\nu}^{-1} d_{l'\kappa'}^{0\kappa}$, and $D \equiv D_{l'\kappa'}^{0\kappa} = \sqrt{[\mathbf{d}_{l'\kappa'}^{0\kappa}]^T \Delta_{l'\kappa'}^{0\kappa}}$, and further define for Eq. (5a): $F_0(\mathbf{K}) = e^{-\epsilon^\infty(\mathbf{K})/4\Lambda^2} / \epsilon^\infty(\mathbf{K})$, with $\epsilon^\infty(\mathbf{K}) = \sum_{\mu\nu} K_\mu \epsilon_{\mu\nu}^\infty K_\nu$. The unit cell volume is Ω_0 and the function $H_{\mu\nu}(\mathbf{x}, y)$ is given by [92]

$$\begin{aligned} H_{\mu\nu}(\mathbf{x}, y) &= \frac{x_\mu x_\nu}{y^2} \left[\frac{3 \operatorname{erfc} y}{y^3} + \frac{2e^{-y^2}}{\sqrt{\pi}} \left(\frac{3}{y^2} + 2 \right) \right] \\ &\quad - (\epsilon^\infty)_{\mu\nu}^{-1} \left[\frac{\operatorname{erfc} y}{y^3} + \frac{2}{\sqrt{\pi}} \frac{e^{-y^2}}{y^2} \right]. \end{aligned} \quad (6)$$

The short-ranged FCs are calculated from the short-ranged part of the dynamical matrices by inverse Fourier transform from reciprocal to real space [92]:

$$\begin{aligned} \text{sr}C_{l'\kappa'\nu}^{0\kappa\mu} &= \frac{1}{N_{\mathbf{q}}} \sum_{\mathbf{q}_i \in \mathcal{G}} \text{sr}\tilde{C}_{\kappa'\nu}^{\kappa\mu}(\mathbf{q}_i) e^{-i\mathbf{q}_i^T \mathbf{R}_{l'}}, \quad \text{if } \mathbf{d}_{l'\kappa'}^{0\kappa} \in \text{box} \\ &= 0, \quad \text{if } \mathbf{d}_{l'\kappa'}^{0\kappa} \notin \text{box}. \end{aligned} \quad (7)$$

The “box” is the volume of size $N_{\mathbf{q}} \times \Omega_0$ in real space (centered on atom κ) containing $N_{\mathbf{q}}$ lattice points $\mathbf{R}_{l'}$ at which the short-ranged FCs are obtained. We reiterate at this point that these FCs now are supposed to be sufficiently short ranged (decaying at least as $|\mathbf{d}_{l'\kappa'}^{0\kappa\mu}|^{-4}$) making the Fourier sum more rapidly convergent [first term of Eq. (3)] compared to the case when the full FCs are used [Eq. (2)] [92].

Now that the short-ranged FCs have been obtained, full dynamical matrices at *any* point in the BZ (i.e., in particular at points *not* contained in the original grid \mathcal{G}) can be calculated by Fourier interpolation. For an arbitrary \mathbf{q} vector the interpolation procedure [implementing Eq. (3)] can be summarized as follows:

(I) Calculate the first term of Eq. (3) with the short-ranged FCs ${}^{\text{sr}}C_{l'\kappa'}^{0\kappa\mu}$ to obtain the short-ranged dynamical matrix ${}^{\text{sr}}\tilde{C}_{\kappa'\nu}^{\kappa\mu}(\mathbf{q})$.

(II) Calculate the dipole-dipole part ${}^{\text{dd}}\tilde{C}_{\kappa'\nu}^{\kappa\mu}(\mathbf{q})$ [second term of Eq. (3)] according to Eqs. (5).

(III) Complete the instruction of Eq. (3): Add the dipole-dipole part ${}^{\text{dd}}\tilde{C}_{\kappa'\nu}^{\kappa\mu}(\mathbf{q})$ and the short-ranged part ${}^{\text{sr}}\tilde{C}_{\kappa'\nu}^{\kappa\mu}(\mathbf{q})$ in reciprocal space to obtain the full dynamical matrix $\tilde{C}_{\kappa'\nu}^{\kappa\mu}(\mathbf{q})$.

(IV) Calculate phonon frequencies ($\omega_{m\mathbf{q}}$) and eigenvectors ($w_{m\mathbf{q}}^{\kappa\mu}$) for the m th branch by solving the eigenvalue equation of $\tilde{D}_{\kappa'\nu}^{\kappa\mu}(\mathbf{q}) = \tilde{C}_{\kappa'\nu}^{\kappa\mu}(\mathbf{q})/(M_{\kappa}M_{\kappa'})^{1/2}$:

$$\sum_{\kappa'\nu} \tilde{D}_{\kappa'\nu}^{\kappa\mu}(\mathbf{q}) w_{m\mathbf{q}}^{\kappa'\nu} = (\omega_{m\mathbf{q}})^2 w_{m\mathbf{q}}^{\kappa\mu}. \quad (8)$$

Since the approach we just reviewed “corrects” the shortcomings of the Fourier interpolation based on the full FCs, we refer to it as *dipole-dipole corrections*.

As a final point of this section we note that the term corresponding to $\mathbf{G} = \mathbf{0}$ in Eq. (5a), after having included the Born effective charges like in Eq. (5b), leads to the nonanalytical term that appears in the $\mathbf{q} \rightarrow \mathbf{0}$ limit of the dipole-dipole part of the dynamical matrix along direction $\hat{\mathbf{q}}$ [90,92]:

$${}^{\text{na}}\tilde{C}_{\kappa'\nu}^{\kappa\mu}(\hat{\mathbf{q}}) = \frac{4\pi}{\Omega_0} \frac{\sum_{\mu'\nu'} \hat{q}_{\mu'} Z_{\kappa,\mu'\mu}^* \sum_{\nu''} \hat{q}_{\nu''} Z_{\kappa',\nu''\nu}}{\epsilon^{\infty}(\hat{\mathbf{q}})}. \quad (9)$$

This term describes a macroscopic electric field [96,99] which—due to the imposition of periodic boundary conditions—is not captured in DFT calculations. Therefore, for a given direction $\hat{\mathbf{q}}$, this term must be added explicitly to the full dynamical matrix:

$$\lim_{\mathbf{q} \rightarrow \mathbf{0}} \tilde{C}_{\kappa'\nu}^{\kappa\mu}(\mathbf{q}) = \tilde{C}_{\kappa'\nu}^{\kappa\mu}(\mathbf{q} = \mathbf{0}) + {}^{\text{na}}\tilde{C}_{\kappa'\nu}^{\kappa\mu}(\hat{\mathbf{q}}). \quad (10)$$

B. The method of Gonze and Lee in the framework of the direct method

In Sec. II A we have reviewed the method of Gonze and Lee [92] in relation to DFPT. The key requirement for this method to be applicable is that full dynamical matrices $\{\tilde{C}_{\kappa'\nu}^{\kappa\mu}(\mathbf{q}_i)\}_{i=1,\dots,N_{\mathbf{q}}}$ are known for a set of wave vectors that homogeneously sample the BZ.

The purpose of this section is to show how this procedure [92] can be used in conjunction with the direct method. This method [87–89] is used in this article to compute FCs in

combination with DFT calculations (note that we are *not* using DFPT to determine the FCs).

The direct method relies on systematically displacing an atom κ' in unit cell l' by a finite amount from its equilibrium position in a supercell and calculating resultant Hellman-Feynman forces from DFT on another atom κ in the $l = 0$ unit cell at the origin. From these forces we compute the FCs using a two-point finite difference stencil.

The peculiarity of the FCs based on DFT calculations is that they are determined from forces having contributions from displaced atoms in all periodic images of the supercell. This is due to periodic boundary conditions imposed in most DFT codes [97,98,100–103]. Through the forces the periodic contributions enter the FCs which is the reason why these are often termed cumulative FCs [88]: $C_{l'\kappa'}^{0\kappa\mu} = \sum_{l'} {}^{\text{phy}}C_{l'+Ll'\kappa'}^{0\kappa\mu}$, where the summation extends over all periodic images of the supercell, and ${}^{\text{phy}}C_{l'\kappa'}^{0\kappa\mu}$ are the true physical force constants. At wave vectors $\mathbf{q}_{\mathbf{c}}$ that are reciprocal lattice vectors of the real space superlattice, the full dynamical matrix can be obtained exactly without any further approximation [88,104]. For these wave vectors commensurable with the supercell it holds that $e^{+i\mathbf{q}_{\mathbf{c}}\cdot\mathbf{R}_L^{(s)}} = 1$ since $\mathbf{q}_{\mathbf{c}}^T \mathbf{R}_L^{(s)} = 2\pi \times \text{integer}$, $\mathbf{R}_L^{(s)}$ being a lattice vector of the real space superlattice. Therefore, using the FCs $C_{l'\kappa'}^{0\kappa\mu}$ in Eq. (2), exact full dynamical matrices $\tilde{C}_{\kappa'\nu}^{\kappa\mu}(\mathbf{q}_{\mathbf{c}})$ at the commensurable wave vectors are obtained.

The $\mathbf{q}_{\mathbf{c}}$ vectors can be generated in the following way: Let $\mathbf{a}_1^{(p)}, \mathbf{a}_2^{(p)}, \mathbf{a}_3^{(p)}$ and $\mathbf{a}_1^{(s)}, \mathbf{a}_2^{(s)}, \mathbf{a}_3^{(s)}$ be the generating vectors of the real space unit- and superlattice, respectively. The two are related by a linear transformation $\sum_{j=1}^3 \mathbf{a}_j^{(p)} M_{jj'} = \mathbf{a}_{j'}^{(s)}$, with $M \in \mathbb{Z}^{3 \times 3}$. The columns of the reciprocal of the transformation matrix $[M^T]^{-1} \in \mathbb{Q}^{3 \times 3}$ can be taken as generating vectors for a grid $\mathcal{G}_{\mathbf{c}}$ of $\mathbf{q}_{\mathbf{c}}$ vectors of size $N_{\mathbf{q}_{\mathbf{c}}} = \det M$. Note that, using these generating vectors, the $\mathbf{q}_{\mathbf{c}}$ vectors refer to the basis of the reciprocal lattice corresponding to the lattice generated by $\mathbf{a}_1^{(p)}, \mathbf{a}_2^{(p)}, \mathbf{a}_3^{(p)}$ in real space.

Since we have access to exact full dynamical matrices on a grid $\mathcal{G}_{\mathbf{c}}$ of wave vectors (which now plays the role of \mathcal{G} from Sec. II A), we are now in the position to apply the method of Gonze and Lee [92] within the framework of the direct method. Assuming that the (cumulative) FCs $C_{l'\kappa'}^{0\kappa\mu}$ have already been calculated from a supercell with volume $N_{\mathbf{q}_{\mathbf{c}}} \times \det(\mathbf{a}_1^{(p)}, \mathbf{a}_2^{(p)}, \mathbf{a}_3^{(p)}) = N_{\mathbf{q}_{\mathbf{c}}} \times \Omega_0$, the essential steps can be summarized in the following way ($\mathbf{q}_{\mathbf{c}}$ replaces \mathbf{q}_i in the equations from Sec. II A):

(i) $\forall \mathbf{q}_{\mathbf{c}} \in \mathcal{G}_{\mathbf{c}}$: Use the (cumulative) FCs $C_{l'\kappa'}^{0\kappa\mu}$ in Eq. (2) to calculate the exact full dynamical matrices $\tilde{C}_{\kappa'\nu}^{\kappa\mu}(\mathbf{q}_{\mathbf{c}})$.

(ii) $\forall \mathbf{q}_{\mathbf{c}} \in \mathcal{G}_{\mathbf{c}}$: Calculate the dipole-dipole part ${}^{\text{dd}}\tilde{C}_{\kappa'\nu}^{\kappa\mu}(\mathbf{q}_{\mathbf{c}})$ [Eqs. (5)] and remove it from the exact full dynamical matrices $\tilde{C}_{\kappa'\nu}^{\kappa\mu}(\mathbf{q}_{\mathbf{c}})$ [following Eq. (4)] to obtain the short-ranged part ${}^{\text{sr}}\tilde{C}_{\kappa'\nu}^{\kappa\mu}(\mathbf{q}_{\mathbf{c}})$.

(iii) Construct the short-ranged FCs ${}^{\text{sr}}C_{l'\kappa'}^{0\kappa\mu}$ in real space by inverse Fourier transform like in Eq. (7).

(iv) To interpolate to arbitrary \mathbf{q} vectors, follow items (I) to (IV) for the Fourier interpolation described in Sec. II A.

In relation with the direct method, Wang *et al.* [105] have proposed another method for the inclusion of dipole-dipole corrections into dynamical matrices. Contrary to the approach

followed here, in Wang's method the Fourier interpolation is carried out with the full FCs and subsequent addition of the nonanalytic term from Eq. (9) times a wave-vector-dependent factor [105,106]. Wang's method has often been used in recent years in conjunction with the direct method [13,105–114], and has been implemented into many phonon codes [98,113,115–118]. As also pointed out by Wang *et al.* [119], both methods are quite different only from a technical point of view, particularly in their treatment of the Fourier interpolation. We found the differences in the overall phonon dispersion to be quite small in cases of Cu₂O and Cu₄O₃. For monoclinic CuO, differences are more clearly visible and differences cannot be ruled out for other materials. A detailed comparative study shall, however, not be subject of the present work.

C. Calculation of first-order derivatives of phonon mode frequencies in the limit $\mathbf{q} \rightarrow \mathbf{0}$

In discussing the properties of the eigenvalue problem Eq. (8) for polar solids in the limit $\mathbf{q} \rightarrow \mathbf{0}$, seminal work has been done by Born and Huang [99] (Chap. V). We rewrite parts of their procedure for the treatment of long-wavelength acoustic phonons in the presence of dipole-dipole interactions (also discussed in great detail in Ref. [96]) for the case of anisotropic dielectric permittivity and Born effective charge tensors, introduced by Gonze and Lee [92].

To keep in line with [96,99], we consider the following change-of-phase for the full dynamical matrix:

$$\tilde{\mathcal{E}}_{\kappa'v}^{\kappa\mu}(\mathbf{q}) = e^{+i\mathbf{q}^T \mathbf{x}_{\kappa'}} \tilde{\mathcal{C}}_{\kappa'v}^{\kappa\mu}(\mathbf{q}) e^{-i\mathbf{q}^T \mathbf{x}_{\kappa}}. \quad (11)$$

This phase change of the dynamical matrix can be advantageous for discussing relations between the FCs and the macroscopic elastic constants (see [96], Chaps. 2 and 6).

In order to develop the equations governing the $\mathbf{q} \rightarrow \mathbf{0}$ limit of the phonon mode frequencies, we will work with the mass-reduced full dynamical matrix $\tilde{\mathcal{D}}_{\kappa'v}^{\kappa\mu}(\mathbf{q}) = \tilde{\mathcal{E}}_{\kappa'v}^{\kappa\mu}(\mathbf{q}) / (M_{\kappa} M_{\kappa'})^{1/2}$ whose eigenvalues and eigenvectors we shall denote by $(\omega_{m\mathbf{q}})^2$ and $b_{m\mathbf{q}}^{\kappa\mu}$, respectively.

Next, for fixed direction $\hat{\mathbf{q}}$, we expand the single parts of the corresponding eigenvalue equation [cf. Eq. (8)] around $\mathbf{q} = \mathbf{0}$ (letting $\lambda = |\mathbf{q}|$):

$$\tilde{\mathcal{D}}_{\kappa'v}^{\kappa\mu} = \tilde{\mathcal{D}}_{0,\kappa'v}^{\kappa\mu} + \text{na} \tilde{\mathcal{D}}_{1,\kappa'v}^{\kappa\mu} + i \tilde{\mathcal{D}}_{1,\kappa'v}^{\kappa\mu} \lambda + \frac{1}{2} \tilde{\mathcal{D}}_{2,\kappa'v}^{\kappa\mu} \lambda^2 + \dots, \quad (12a)$$

$$b_{m\mathbf{q}}^{\kappa\mu} = b_{0,m}^{\kappa\mu} + i b_{1,m}^{\kappa\mu} \lambda + \frac{1}{2} b_{2,m}^{\kappa\mu} \lambda^2 + \dots, \quad (12b)$$

$$\omega_{m\mathbf{q}} = \omega_{1,m} \hat{\mathbf{q}} \lambda + \frac{1}{2} \omega_{2,m} \hat{\mathbf{q}} \lambda^2 + \dots, \quad (12c)$$

wherein $\text{na} \tilde{\mathcal{D}}_{1,\kappa'v}^{\kappa\mu} \equiv \text{na} \tilde{\mathcal{D}}_{1,\kappa'v}^{\kappa\mu}(\hat{\mathbf{q}}) = \text{na} \tilde{\mathcal{E}}_{1,\kappa'v}^{\kappa\mu}(\hat{\mathbf{q}}) / (M_{\kappa} M_{\kappa'})^{1/2}$, and the $\mathbf{q} = \mathbf{0}$ label has been suppressed in favor of a concise notation.

The parts of the set of Eqs. (12) needed in the following are

$$\tilde{\mathcal{D}}_{0,\kappa'v}^{\kappa\mu} = \text{sr} \tilde{\mathcal{D}}_{0,\kappa'v}^{\kappa\mu} + \text{dd} \tilde{\mathcal{D}}_{0,\kappa'v}^{\kappa\mu}, \quad (13a)$$

$$\tilde{\mathcal{D}}_{1,\kappa'v}^{\kappa\mu} = \sum_{\gamma} (\text{sr} \tilde{\mathcal{D}}_{1,\kappa'v,\gamma}^{\kappa\mu} + \text{dd} \tilde{\mathcal{D}}_{1,\kappa'v,\gamma}^{\kappa\mu}) \hat{q}_{\gamma}, \quad (13b)$$

$$\tilde{\mathcal{D}}_{2,\kappa'v}^{\kappa\mu} = \sum_{\gamma\lambda} (\text{sr} \tilde{\mathcal{D}}_{2,\kappa'v,\gamma\lambda}^{\kappa\mu} + \text{dd} \tilde{\mathcal{D}}_{2,\kappa'v,\gamma\lambda}^{\kappa\mu}) \hat{q}_{\gamma} \hat{q}_{\lambda}, \quad (13c)$$

and

$$\omega_{1,m\hat{\mathbf{q}}} = \sum_{\gamma} \left. \frac{\partial \omega_{m\mathbf{q}}}{\partial q_{\gamma}} \right|_{\mathbf{q}=\mathbf{0}} \hat{q}_{\gamma}, \quad (14a)$$

$$b_{1,m}^{\kappa\mu} = \sum_{\gamma} \left. \frac{\partial b_{m\mathbf{q}}^{\kappa\mu}}{\partial q_{\gamma}} \right|_{\mathbf{q}=\mathbf{0}} \hat{q}_{\gamma}, \quad (14b)$$

while the derivatives with respect to the wave vector of the short-ranged part of the dynamical matrix at $\mathbf{q} = \mathbf{0}$ read

$$\text{sr} \tilde{\mathcal{D}}_{1,\kappa'v,\gamma}^{\kappa\mu} = \sum_{l'} \frac{\text{sr} \mathcal{C}_{l'\kappa'v}^{0\kappa\mu}}{\sqrt{M_{\kappa} M_{\kappa'}}} d_{l'\kappa'}^{0\kappa}, \quad (15a)$$

$$\text{sr} \tilde{\mathcal{D}}_{2,\kappa'v,\gamma\lambda}^{\kappa\mu} = - \sum_{l'} \frac{\text{sr} \mathcal{C}_{l'\kappa'v}^{0\kappa\mu}}{\sqrt{M_{\kappa} M_{\kappa'}}} d_{l'\kappa',\gamma}^{0\kappa} d_{l'\kappa',\lambda}^{0\kappa}. \quad (15b)$$

The derivatives of the dipole-dipole part require a careful treatment. Starting from a phase-changed version of Eq. (5a), we consider for the further treatment an expression of the form [96,99]

$$\begin{aligned} \text{dd} \tilde{\mathcal{E}}_{\kappa'v}^{\kappa\mu}(\mathbf{q}) &= \frac{4\pi}{\Omega_0} \frac{q_{\mu} q_{\nu}}{\epsilon^{\infty}(\mathbf{q})} (e^{-\epsilon^{\infty}(\mathbf{q})/4\Lambda^2} - 1) \\ &+ \frac{4\pi}{\Omega_0} \sum_{\substack{|\mathbf{G}| \neq 0 \\ \mathbf{K} = \mathbf{q} + \mathbf{G}}} K_{\mu} K_{\nu} F_0(\mathbf{K}) e^{i\mathbf{G}^T (\mathbf{x}_{\kappa} - \mathbf{x}_{\kappa'})} \\ &- \sum_{l', D \neq 0} \Lambda^3 H_{\mu\nu}(\Lambda \Delta, \Lambda D) \frac{e^{i\mathbf{q}^T \mathbf{d}_{l'\kappa'}^{0\kappa}}}{\sqrt{\det \epsilon^{\infty}}} \\ &- \frac{4}{3\sqrt{\pi}} \frac{\Lambda^3}{\sqrt{\det \epsilon^{\infty}}} \delta_{\kappa\kappa'} (\epsilon^{\infty})_{\mu\nu}^{-1}, \end{aligned} \quad (16)$$

which possesses a unique limiting value at vanishing wave vector. The Born effective charges must be included in the first- and second-order derivatives of the dipole-dipole part:

$$\begin{aligned} \text{dd} \tilde{\mathcal{D}}_{1,\kappa'v,\gamma}^{\kappa\mu} &= \sum_{\mu'v'} Z_{\kappa,\mu'}^* Z_{\kappa',v'}^* \\ &\times \lim_{\mathbf{q} \rightarrow \mathbf{0}} \text{dd} \tilde{\mathcal{E}}_{1,\kappa'v,\gamma}^{\kappa\mu'}(\mathbf{q}) / (M_{\kappa} M_{\kappa'})^{1/2}, \end{aligned} \quad (17a)$$

$$\begin{aligned} \text{dd} \tilde{\mathcal{D}}_{2,\kappa'v,\gamma\lambda}^{\kappa\mu} &= \sum_{\mu'v'} Z_{\kappa,\mu'}^* Z_{\kappa',v'}^* \\ &\times \lim_{\mathbf{q} \rightarrow \mathbf{0}} \text{dd} \tilde{\mathcal{E}}_{2,\kappa'v,\gamma\lambda}^{\kappa\mu'}(\mathbf{q}) / (M_{\kappa} M_{\kappa'})^{1/2}, \end{aligned} \quad (17b)$$

with $\text{dd} \tilde{\mathcal{E}}_{1,\kappa'v,\gamma}^{\kappa\mu}(\mathbf{q}) = -i \frac{\partial}{\partial q_{\gamma}} \text{dd} \tilde{\mathcal{E}}_{\kappa'v}^{\kappa\mu}(\mathbf{q})$, $\text{dd} \tilde{\mathcal{E}}_{2,\kappa'v,\gamma\lambda}^{\kappa\mu}(\mathbf{q}) = \frac{\partial^2}{\partial q_{\lambda} \partial q_{\gamma}} \text{dd} \tilde{\mathcal{E}}_{\kappa'v}^{\kappa\mu}(\mathbf{q})$. Mind that the factor $-i$ in the first derivative has been included because a factor $+i$ was introduced in the term linear in λ of Eq. (12a). Upon carefully performing the

limits the result is

$$\text{dd}\bar{\mathcal{G}}_{1,\kappa'\nu,\gamma}^{\kappa\mu} = -\frac{4\pi i}{\Omega_0} \sum_{|\mathbf{G}|\neq 0} e^{i\mathbf{G}^T(\mathbf{x}_\kappa - \mathbf{x}_{\kappa'})} [(\delta_{\mu\gamma} G_\nu + G_\mu \delta_{\nu\gamma}) F_0(\mathbf{G}) + G_\mu G_\nu (\epsilon^\infty \mathbf{G})_\gamma F_1(\mathbf{G})] - \sum_{l', D \neq 0} \frac{\Lambda^3}{\sqrt{\det \epsilon^\infty}} H_{\mu\nu}(\Lambda \mathbf{\Delta}, \Lambda D) d_{l'\kappa',\gamma}^{0\kappa}, \quad (18a)$$

$$\begin{aligned} \text{dd}\bar{\mathcal{G}}_{2,\kappa'\nu,\gamma\lambda}^{\kappa\mu} &= -\frac{4\pi}{\Omega_0} (4\Lambda^2)^{-1} (\delta_{\mu\gamma} \delta_{\nu\lambda} + \delta_{\mu\lambda} \delta_{\nu\gamma}) + \frac{4\pi}{\Omega_0} \sum_{|\mathbf{G}|\neq 0} e^{i\mathbf{G}^T(\mathbf{x}_\kappa - \mathbf{x}_{\kappa'})} [(\delta_{\mu\gamma} \delta_{\nu\lambda} + \delta_{\mu\lambda} \delta_{\nu\gamma}) F_0(\mathbf{G}) \\ &+ (\delta_{\mu\lambda} G_\nu + G_\mu \delta_{\nu\lambda}) (\epsilon^\infty \mathbf{G})_\gamma F_1(\mathbf{G}) + (\delta_{\mu\gamma} G_\nu + G_\mu \delta_{\nu\gamma}) (\epsilon^\infty \mathbf{G})_\lambda F_1(\mathbf{G}) \\ &+ G_\mu G_\nu \epsilon^\infty_{\gamma\lambda} F_1(\mathbf{G}) + G_\mu G_\nu (\epsilon^\infty \mathbf{G})_\gamma (\epsilon^\infty \mathbf{G})_\lambda F_2(\mathbf{G})] + \sum_{l', D \neq 0} \frac{\Lambda^3}{\sqrt{\det \epsilon^\infty}} H_{\mu\nu}(\Lambda \mathbf{\Delta}, \Lambda D) d_{l'\kappa',\gamma}^{0\kappa} d_{l'\kappa',\lambda}^{0\kappa}, \end{aligned} \quad (18b)$$

wherein

$$F_1(\mathbf{K}) = -\frac{2F_0(\mathbf{K})}{4\Lambda^2} - \frac{2F_0(\mathbf{K})}{\epsilon^\infty(\mathbf{K})}, \quad (19a)$$

$$F_2(\mathbf{K}) = -\frac{2F_1(\mathbf{K})}{4\Lambda^2} - \frac{2F_1(\mathbf{K})}{\epsilon^\infty(\mathbf{K})} + \frac{4F_0(\mathbf{K})}{(\epsilon^\infty(\mathbf{K}))^2}. \quad (19b)$$

We now return to the expansions in Eqs. (12) and equate terms of like power in λ up to order λ^2 to arrive at the following set of equations:

$$\sum_{\kappa'\nu} \tilde{\mathcal{D}}_{0,\kappa'\nu}^{\kappa\mu} b_{0,m}^{\kappa'\nu} = -\sum_{\kappa'\nu} \text{na} \tilde{\mathcal{D}}_{0,\kappa'\nu}^{\kappa\mu} b_{0,m}^{\kappa'\nu}, \quad (20a)$$

$$i \sum_{\kappa'\nu} \tilde{\mathcal{D}}_{0,\kappa'\nu}^{\kappa\mu} b_{1,m}^{\kappa'\nu} = -i \sum_{\kappa'\nu} \text{na} \tilde{\mathcal{D}}_{\kappa'\nu}^{\kappa\mu} b_{1,m}^{\kappa'\nu} - i \sum_{\kappa'\nu} \tilde{\mathcal{D}}_{1,\kappa'\nu}^{\kappa\mu} b_{0,m}^{\kappa'\nu}, \quad (20b)$$

$$\begin{aligned} \frac{1}{2} \sum_{\kappa'\nu} \tilde{\mathcal{D}}_{0,\kappa'\nu}^{\kappa\mu} b_{2,m}^{\kappa'\nu} &= (\omega_{1,m\hat{\mathbf{q}}})^2 b_{0,m}^{\kappa\mu} - \frac{1}{2} \sum_{\kappa'\nu} \text{na} \tilde{\mathcal{D}}_{\kappa'\nu}^{\kappa\mu} b_{2,m}^{\kappa'\nu} \\ &+ \sum_{\kappa'\nu} \tilde{\mathcal{D}}_{1,\kappa'\nu}^{\kappa\mu} b_{1,m}^{\kappa'\nu} - \frac{1}{2} \sum_{\kappa'\nu} \tilde{\mathcal{D}}_{2,\kappa'\nu}^{\kappa\mu} b_{0,m}^{\kappa'\nu}. \end{aligned} \quad (20c)$$

Noting that the displacements of the acoustic modes are just a rigid displacement of all atoms, $b_{0,m}^{\kappa\mu} = \sqrt{M_\kappa} u_{0,m}^\mu$, and using the charge neutrality condition $\sum_\kappa Z_\kappa^* \chi_{\kappa,\mu\nu} = 0$, the solution of the first equation (20a) is trivial. We solve Eq. (20b) for the first-order derivatives in the eigenvectors:

$$\begin{aligned} b_{1,m}^{\kappa\mu} &= -\sum_{\kappa'\nu} \sum_{\substack{\kappa_1\kappa_1' \\ \mu_1\mu_1'}} [(\mathbb{1}^\perp + \mathcal{G}^\perp \text{na} \tilde{\mathcal{D}}^\perp)^{-1}]_{\kappa_1\mu_1}^{\kappa\mu} \\ &\times \mathcal{G}_{\kappa_1'\mu_1'}^\perp \tilde{\mathcal{D}}_{1,\kappa_1'\nu}^{\kappa_1\mu_1} \sqrt{M_{\kappa_1'}} u_{0,m}^{\nu}, \end{aligned} \quad (21)$$

where we defined the Green's function of the subspace of optical modes V^\perp ,

$$\mathcal{G}_{\kappa'\nu}^\perp{}^{\kappa\mu} = \sum_{m \in V^\perp} b_{0,m}^{\kappa\mu} [b_{0,m}^{\kappa'\nu}]^* / (\omega_{m\mathbf{q}=0})^2, \quad (22)$$

and the subspace-projected nonanalytical part:

$$\begin{aligned} \text{na} \tilde{\mathcal{D}}_{\kappa'\nu}^\perp{}^{\kappa\mu} &= \sum_{mm' \in V^\perp} b_{0,m}^{\kappa\mu} [b_{0,m'}^{\kappa'\nu}]^* \\ &\times \sum_{\substack{\kappa_1\kappa_1' \\ \mu_1\mu_1'}} [b_{0,m}^{\kappa_1\mu_1}]^* \text{na} \tilde{\mathcal{D}}_{\kappa_1'\mu_1'}^{\kappa_1\mu_1} b_{0,m'}^{\kappa_1'\mu_1'}. \end{aligned} \quad (23)$$

In the context of Eqs. (22) and (23) ($\omega_{m\mathbf{q}=0}$)² and $b_{0,m}^{\kappa\mu}$ shall denote the eigenvalues and eigenvectors of the dynamical matrix in Eq. (13a), respectively. Inserting Eq. (21) into Eq. (20c) we may solve for the first-order derivative of the phonon mode frequencies by following the arguments for the solvability of Eq. (20c) discussed in Chap. 2 of Ref. [96] with the result that

$$\sum_{\nu} [\chi_{\mu\nu} - \delta_{\mu\nu} (\omega_{1,m\hat{\mathbf{q}}})^2] u_{0,m}^\nu = 0, \quad (24)$$

with ($M_0 = \sum_\kappa M_\kappa$) $\chi_{\mu\nu} = M_0^{-1} \sum_{\kappa\kappa'} \sqrt{M_\kappa M_{\kappa'}} \chi_{\kappa'\nu}^{\kappa\mu}$, and

$$\begin{aligned} \chi_{\kappa'\nu}^{\kappa\mu} &= \frac{1}{2} \tilde{\mathcal{D}}_{2,\kappa'\nu}^{\kappa\mu} + \sum_{\substack{\kappa_1\kappa_1' \\ \mu_1\mu_1'}} \tilde{\mathcal{D}}_{1,\kappa_1\mu_1}^{\kappa\mu} \\ &\times [(\mathbb{1}^\perp + \mathcal{G}^\perp \text{na} \tilde{\mathcal{D}}^\perp)^{-1} \mathcal{G}^\perp]_{\kappa_1'\mu_1'}^{\kappa_1\mu_1} \tilde{\mathcal{D}}_{1,\kappa_1'\nu}^{\kappa_1\mu_1'}. \end{aligned} \quad (25)$$

D. Thermodynamics

Within the harmonic approximation the thermodynamic functions can be computed from simple summations over functions of the phonon eigenfrequencies. In this article we compare the vibrational entropy S^{ph} , and the lattice specific heat at constant volume C_v^{ph} , to experimental data from the literature. The expressions for the afore-mentioned quantities at temperature T are ($\hbar \rightarrow 1$, k_B : Boltzmann constant) [96]:

$$\begin{aligned} S^{\text{ph}}(T) &= \frac{k_B}{N_q} \sum_{\mathbf{q},m} \left\{ \frac{\omega_{m\mathbf{q}}}{2k_B T} \coth \left(\frac{\omega_{m\mathbf{q}}}{2k_B T} \right) \right. \\ &\left. - \ln \left[2 \sinh \left(\frac{\omega_{m\mathbf{q}}}{2k_B T} \right) \right] \right\}, \end{aligned} \quad (26)$$

$$C_v^{\text{ph}}(T) = \frac{k_B}{N_q} \sum_{\mathbf{q},m} \frac{\left(\frac{\omega_{m\mathbf{q}}}{2k_B T} \right)^2}{\sinh^2 \left(\frac{\omega_{m\mathbf{q}}}{2k_B T} \right)}. \quad (27)$$

TABLE I. Structural parameters for Cu₂O (GGA), and Cu₄O₃ (GGA + *U* [123]) compared to experimental and calculated values from the literature (Ref. [26]: HSE06, Ref. [85]: LDA + *U*). Ω₀ refers to the unit cell volume.

Phase	Parameter	Present work	Literature	
			Theory	Experiment
Cu ₂ O	<i>a</i> (Å)	4.303	4.2675 [26]	4.2696 [10]
	Cu–O (Å)	1.86	1.85 [26]	1.85 [10]
	Ω ₀ (Å ³)	79.7	77.72 [26]	77.83 [10]
Cu ₄ O ₃	<i>a</i> (Å)	5.873	5.8392 [26], 5.595 [85]	5.837 [124]
	<i>c</i> (Å)	9.990	9.8966 [26], 9.650 [85]	9.932 [124]
	<i>z</i>	0.1146	0.1142 [26], 0.115 [85]	0.1173 [124]
	Cu ⁺ –O ⁽¹⁾ (Å)	1.86	1.85 [26]	1.87 [124]
	Cu ²⁺ –O ⁽²⁾ (Å)	1.93	1.91 [26]	1.92 [124]
	Cu ²⁺ –O ⁽¹⁾ (Å)	2.00	1.98 [26]	1.97 [124]
	Ω ₀ (Å ³)	344.6	337.44 [26], 302.08 [85]	338.39 [124]

Within Debye theory the constant-volume heat capacity per unit cell is [96]

$$C_{v,D}^{\text{ph}}(T) = 9nk_B \left(\frac{T}{\Theta_D} \right)^3 \int_0^{\frac{\Theta_D}{T}} d\xi \frac{\xi^4 e^\xi}{(e^\xi - 1)^2}. \quad (28)$$

Here Θ_D denotes the Debye characteristic temperature, and *n* is the number of atoms in the unit cell. The Debye temperature as a function of *T* is derived by minimizing the residual of calculated (measured) specific heat and Eq. (28) with respect to Θ_D, $\min_{\Theta_D} |C_{v,D}^{\text{ph}}(T) - C_{v,D}^{\text{ph}}(T)|^2$.

E. Computational details

For all our calculations we use the VASP [100–103] code and the therein implemented projector augmented-wave method (PAW) [120,121]. The copper PAW potentials treat the Cu 3*p*⁶, 3*d*¹⁰, and 4*s*¹ electrons as valence electrons while for the O PAW potential the O 2*s*² and 2*p*⁴ electrons are chosen as valence states. For Cu₂O and Cu₄O₃ we use the GGA parametrization for the exchange correlation functional. For the latter case of Cu₄O₃ we additionally apply rotationally invariant Hubbard *U* corrections as suggested by Liechtenstein *et al.* [122]. For monoclinic CuO the LDA + *U* method is used. Any calculation involving Hubbard *U* corrections is conducted with the *ab initio* values of *U* = 7.5 eV and *J* = 0.98 eV that have been determined for a copper oxide system [123].

Literature data for the lattice parameters of CuO based on LDA + *U* [26,85] calculations show deviations of about 2% to 4% from experiment. We therefore use the experimental lattice parameters *a* = 4.6837 Å, *b* = 3.4226 Å, *c* = 5.1288 Å, and β = 99.54° measured by Åsbrink and Norrby [31]. From these the magnetic unit cell for temperatures below *T*_N⁽²⁾ with eight formula units (16 atoms) is constructed [32].

We relax structural parameters only for cubic Cu₂O and tetragonal Cu₄O₃. Calculated values are listed in Table I together with calculated and measured data from the literature. For the structural relaxation a cut-off energy of 1200 eV and an energy tolerance of 10^{−8} eV for the self-consistency are used. In case of Cu₂O 12 **k** points in each direction are selected for the BZ integration while for Cu₄O₃ 8³ **k** points are chosen. The GGA(+*U*) approach reproduces experimental values for structural parameters [10,124] very well for these phases, and

also gives values in good agreement with recent theoretical investigations [26] based on hybrid-DFT (HSE06) methods.

In the case of Cu₂O supercells have been chosen as to give full dynamical matrices on a 5 × 5 × 5 grid of commensurable wave vectors with a displacement length of 0.01 Å and a **k**-point density of 0.2 Å^{−1} for the force calculations [125]. For Cu₄O₃ we calculate FCs from supercells giving full dynamical matrices on a 4 × 4 × 4 grid with a displacement length of 0.03 Å and one **k** point for the force calculations. For CuO we calculate FCs from supercells giving full dynamical matrices on a 3 × 6 × 3 grid with a displacement length of 0.05 Å and one **k** point for the force calculations. Only displacements independent by symmetry are considered for each chemical species. Before constructing the supercells atomic positions are relaxed at an energy cutoff of 800 eV (also used for the supercell calculations of all phases) in structures with internal degrees of freedom (CuO and Cu₄O₃), until the residual forces are smaller than 10^{−5} eV/Å. The number of **k** points are chosen in accordance with the supercell sizes.

Born effective charge and the static dielectric permittivity tensors, as needed for the dipole-dipole part of the dynamical matrix, are computed from DFPT as implemented in VASP. The energy cutoff and energy tolerance are the same as for the supercell calculations. For the BZ integration we choose 16³ **k** points for Cu₂O, 10³ **k** points for Cu₄O₃, and 8 × 16 × 8 **k** points in the case of CuO.

III. RESULTS AND DISCUSSION

A. Phonon band structure and density of states

Figure 1 overviews the phonon density of states (PDOS) and phonon band structure for all three copper oxide phases. Dipole-dipole corrections have been invoked in all cases. The particular influence of the latter on the phonon dispersion will be discussed in more detail below.

The PDOS for cubic Cu₂O, tetragonal Cu₄O₃, and monoclinic CuO display quite distinct features. The PDOS of Cu₂O [lower panel of Fig. 1(a)] is dominated by the large gap between the copper and the oxygen states. Contrary to CuO, the low-lying (below ~120 cm^{−1}) Cu-related modes in Cu₂O and Cu₄O₃ produce sharp features in the density of states. Monoclinic CuO [lower panel of Fig. 1(c)], however, shows a

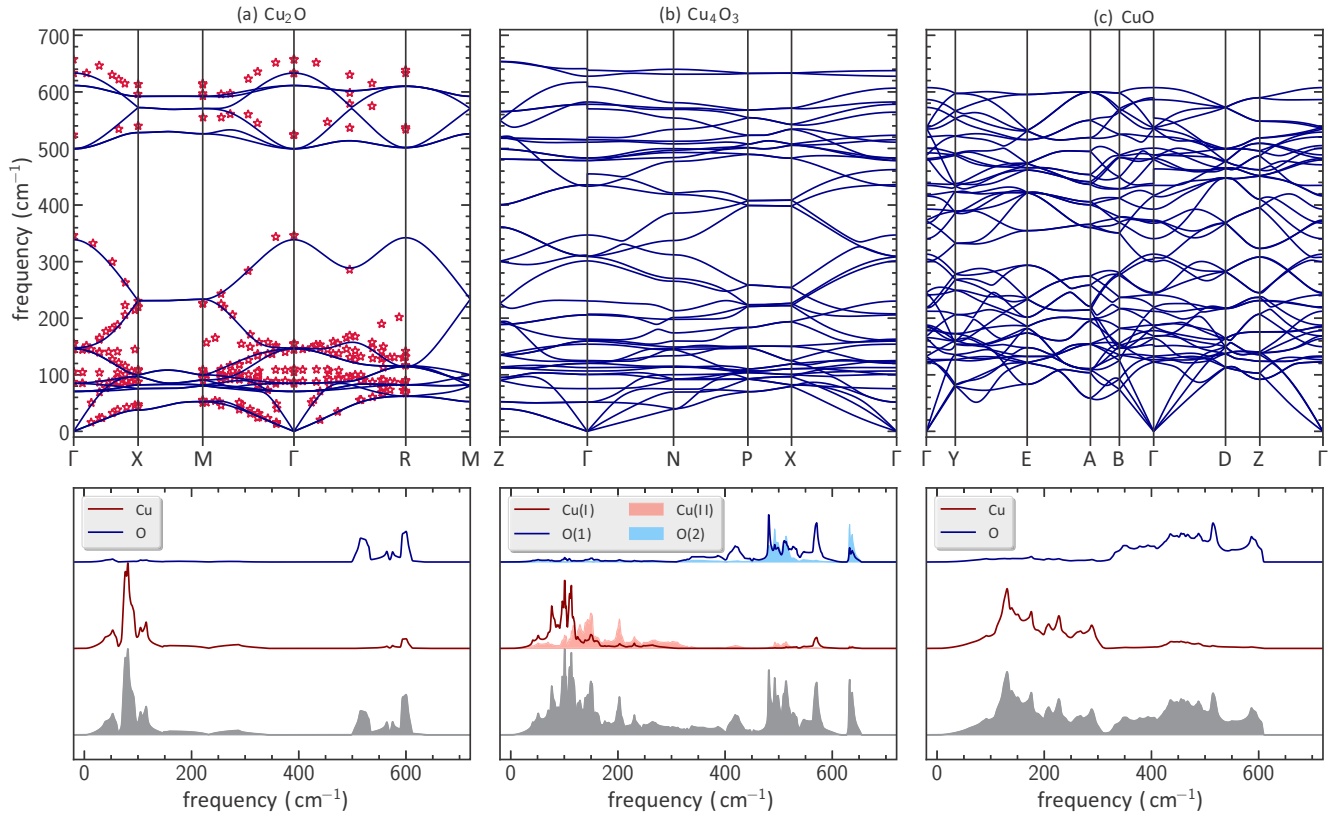


FIG. 1. Phonon band structures (upper panel) and phonon density of states (lower panel) for (a) Cu_2O , (b) Cu_4O_3 , and (c) CuO . Experimental data for Cu_2O (red-bounded stars) is extracted from figures in Ref. [66], and—apart from the latter reference—covers Refs. [60,126]. For simplicity, different references are not distinguished through use of different colors or symbols in the plot.

smoothly increasing PDOS below 100 cm^{-1} resulting from the steep dispersion of the acoustic modes before also displaying a (moderately) peaked structure at higher frequencies than the other two phases. As also discussed in Ref. [42], the difference in magnitude of the FCs for Cu(I) and Cu(II) atoms in the paramelaconite phase becomes very obvious from the different frequency regions the magnetic [Cu(II)] and nonmagnetic [Cu(I)] copper atoms contribute to in the PDOS.

In Fig. 1(a), for Cu_2O , we have included experimental phonon frequencies from the literature [60,66,126]. Agreement between calculated and measured values is excellent, particularly for the low-lying copper-driven modes. The high-frequency, oxygen-related modes, on the contrary, are placed systematically too low (~ 10 to 20 cm^{-1}) compared to experiment—a fact previously observed for GGA calculations [66,95].

In the following we shall discuss the influence of dipole-dipole corrections on the band structure of the three copper oxide phases. For the sake of simplicity, bands subject to changes due to employment of these corrections are labeled according to the symmetry representation of the *purely transverse* mode at the Γ point. This means that, for some particular band on some path directed towards $\mathbf{q} = \mathbf{0}$, we will always refer to the Γ -point symmetry which, in general, will not coincide with the symmetry of this direction. Bands that are influenced by the dipole-dipole corrections establish the infrared-active modes at the BZ center.

Figure 2 displays phonon frequencies with and without dipole-dipole corrections for all copper oxide phases along selected directions in reciprocal space. Frequencies *without* dipole-dipole corrections are related to the eigenvalues of full dynamical matrices from the Fourier transform in Eq. (2) calculated with full FCs $C_{l'k'v}^{0\kappa\mu}$, instead of using Eq. (3).

For cubic Cu_2O there are two infrared-active T_{1u} modes. However, we only consider the high-frequency $T_{1u}^{(2)}$ mode along the $\Gamma \rightarrow X$ direction. The splitting is 22 cm^{-1} for the $T_{1u}^{(2)}$ mode at 611 cm^{-1} opposed to 1.4 cm^{-1} for the $T_{1u}^{(1)}$ at 146.1 cm^{-1} [not shown in Fig. 2(a)]. This is in reasonable agreement with calculated and measured values [64,66]. Owing to cubic symmetry the limiting value for $\mathbf{q} \rightarrow \mathbf{0}$ of the LO mode is the same for all directions.

The representations of the infrared-active modes for tetragonal Cu_4O_3 at the Γ point are (D_{4h} point group) $5A_{2u} \oplus 8E_u$ while for monoclinic CuO they read (C_{2h} point group) $5A_u \oplus 4B_u$. For these phases, due to noncubic symmetry, the frequencies of the modes depend on the direction for which the wave vector approaches zero. Figures 2(b) and 2(c) show magnified band structures along the $\Gamma \rightarrow Z$ and the $\Gamma \rightarrow Y$ directions for Cu_4O_3 and CuO , respectively. In the case of Cu_4O_3 the $A_{2u}^{(4)}$ mode is of strong longitudinal character resulting in a deviation of $\sim 50 \text{ cm}^{-1}$ from the purely transversal mode. For CuO the two longitudinal B_u modes strongly couple to the direction leading to splittings between TO and LO mode of $\sim 20 \text{ cm}^{-1}$ ($B_u^{(3)}$) and $\sim 70 \text{ cm}^{-1}$ ($B_u^{(4)}$).

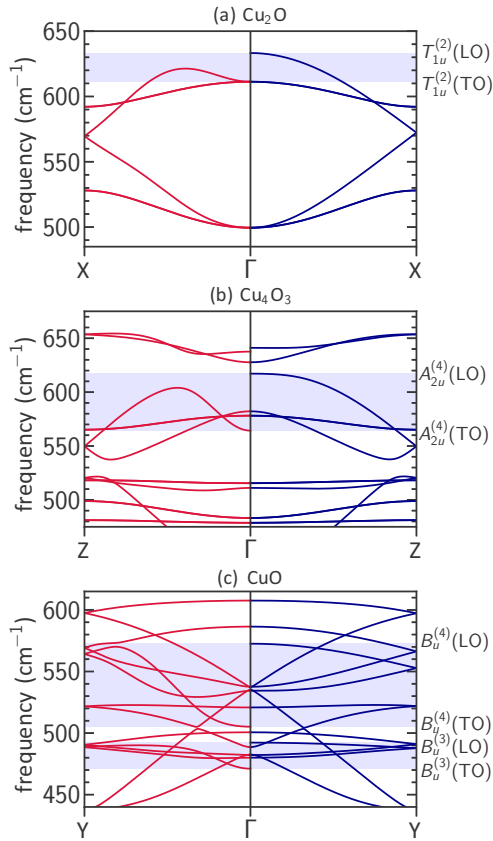


FIG. 2. Phonon band structure along selected directions in reciprocal space for (a) Cu_2O , (b) Cu_4O_3 , and (c) CuO . Dispersions are shown without (red; left to Γ) and with dipole-dipole corrections (dark blue; right to Γ). Shaded areas mark the frequency range bounded by the LO and TO components of the respective mode at the Γ point (see indication of the irreducible representation on the right). Note that only modes subject to clearly visible changes due to the dipole-dipole corrections have been indicated.

From these figures it is clear that neglecting dipole-dipole corrections will lead to grossly erroneous evolution of some bands in the region around $\mathbf{q} = \mathbf{0}$.

We close this section with some final remarks on the role of dipole-dipole corrections in band structures of polar insulators. We have seen from Fig. 2 that, as the wave vector approaches the BZ center, the LO branch of the mode subject to splitting of LO and TO components is deficiently described through full dynamical matrices computed from the full FCs ($C_{\nu'\kappa'\nu}^{0\kappa\mu}$). If the interaction range of these FCs is sufficiently large, the summation in Eq. (2) contains enough terms as to be convergent. In this case, the LO branch, apart from the very vicinity of $\mathbf{q} = \mathbf{0}$, would be congruent with the one calculated including dipole-dipole corrections. In order to exemplify this, consider Fig. 3 where we show the dispersion relation of Cu_2O along the $\Gamma \rightarrow \text{X}$ direction together with phonon frequencies at \mathbf{q}_c vectors commensurate with a $13 \times 1 \times 1$ supercell. At these wave vectors the full dynamical matrices are exact (and hence are the frequencies) since, through the imposed periodic boundary conditions, interactions in Eq. (2) are summed to infinity. Note that attaining these frequencies requires no corrections to be applied to the respective full

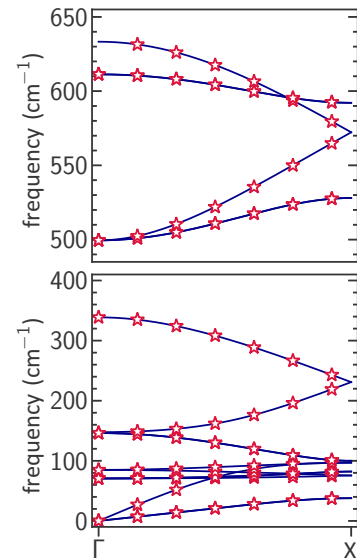


FIG. 3. Phonon band structure of Cu_2O (blue solid line) along the $\Gamma \rightarrow \text{X}$ direction together with phonon frequencies at \mathbf{q}_c vectors commensurate with a $13 \times 1 \times 1$ supercell (red-bordered stars). Note that, among the frequencies at the commensurate wave vectors, the topmost frequency at the Γ point ($\sim 630 \text{ cm}^{-1}$) is not missing but coincides with the frequency directly below ($\sim 610 \text{ cm}^{-1}$). The reason is that the highest-frequency $\mathbf{q} = \mathbf{0}$ phonon mode is accompanied by a macroscopic electric field which is incommensurate with periodic boundary conditions imposed in DFT calculations.

dynamical matrices. The fact that the interpolated frequencies calculated with dipole-dipole corrections enforced for the full dynamical matrices perfectly match the exact frequencies, may be taken as an *a posteriori* confirmation that the method due to Gonze and Lee [92] works in combination with the direct method.

B. Thermodynamic functions

Figure 4 shows our results for the constant-volume lattice specific heat [Eq. (27)] and the vibrational contribution to the entropy [Eq. (26)]. To the best of our knowledge, experimental data so far is only available for Cu_2O [127] and CuO [70,131].

Experimental values for the constant-pressure heat capacity (C_p) of Cu_2O have been corrected in order to obtain the heat capacity at constant volume (C_v) from the relation $C_p - C_v = VT\alpha^2/\beta_T$ (V : sample volume; α : coefficient of thermal expansion; β_T : isothermal compressibility) using the data of Refs. [128–130]. We find good agreement with experiment. The small overestimate of C_v^{ph} and S^{ph} for most temperatures might be due to the slightly overestimated lattice constant through the GGA exchange-correlation functional.

Experimentally, the heat capacity of monoclinic CuO has been studied extensively and also the magnetic contributions have been assessed [70,131–135]. Since our crystal structure in combination with the magnetic ordering is only valid in the low-temperature region, we shall limit our comparison to temperatures below the antiferromagnetic commensurate to incommensurate transition at $T_N^{(2)} = 213 \text{ K}$ [32]. Figure 4 shows our calculated results for the lattice heat capacity and

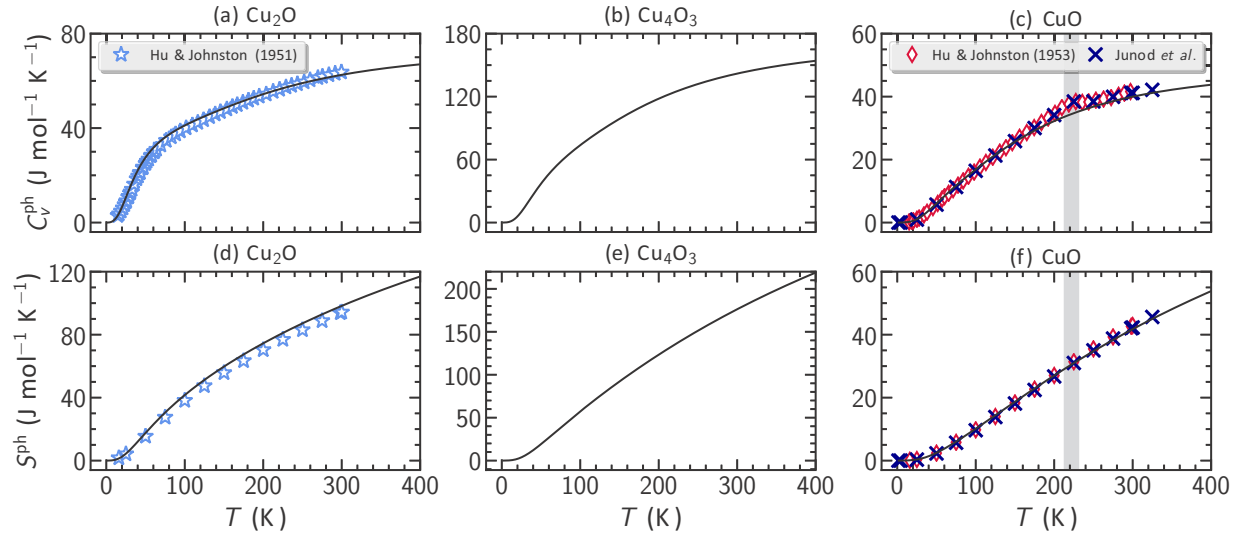


FIG. 4. Constant-volume lattice specific heat (a)–(c) and lattice contribution to entropy (d)–(f) for all three copper oxide phases. Experimental values in (a) for the constant-pressure heat capacity (C_p), and in (d) for the entropy of Cu_2O have been taken from Hu and Johnston [127] (blue stars). Constant-volume heat capacities (C_v) are derived from the relation $C_p - C_v = VT\alpha^2/\beta_T$ (V : sample volume; α : coefficient of thermal expansion; β_T : isothermal compressibility) using the data of Refs. [128–130]. In (c) and (f), in order to get C_v , experimental C_p vs T data for CuO from Refs. [70,131] have been modified following the procedure of Loram *et al.* [132]. The boundaries of the gray-shaded regions in (c) and (f) mark the antiferromagnetic phase transitions characterized by temperatures $T_N^{(1,2)}$.

entropy compared to experimental data from Hu and Johnston [131] and Junod *et al.* [70]. In order to extract the heat capacity at constant volume from the C_p vs T data, a scheme proposed in Ref. [132] has been applied. Agreement between calculated and measured values for the specific heat is excellent up to the anomaly in the experimental curve that coincides with the first antiferromagnetic phase transition [70,131,132,134,135]. For the entropy the agreement prevails up to even higher temperatures.

From the lattice heat capacities at constant volume we extract the Debye characteristic temperatures Θ_D for different temperatures T as previously described in Sec. II D. The results for all three phases are depicted in Fig. 5. For Cu_2O measured values for the heat capacities (see also Fig. 4) have been used to extract the experimental Debye temperatures vs temperature. Agreement with experimental data again is good for both aforementioned phases.

C. Velocities of sound

Acoustic phonon group velocities are related to the first-order derivative of the phonon dispersion through $v_{m\hat{q}}^{\text{sound}} = \omega_{1,m\hat{q}} = \sum_{\gamma} \partial\omega_{m\hat{q}}/\partial q_{\gamma}|_{q=0}\hat{q}_{\gamma}$. For a chosen direction \hat{q} the latter quantity is accessible by solving the 3×3 eigenvalue problem Eq. (24). By m we label the mode polarization as (mainly) transversal (t) or longitudinal (l). This is quantified by projecting the (normalized) center-of-mass displacement per unit cell $\tilde{u}_{m\hat{q}}^{\mu} = M_0^{-1} \sum_{\kappa} M_{\kappa} u_{m\hat{q}}^{\kappa\mu}$ on the direction \hat{q} : $\sum_{\mu} \hat{q}_{\mu} \tilde{u}_{m\hat{q}}^{\mu}$. Therein $\hat{u}_{m\hat{q}}^{\mu} = \tilde{u}_{m\hat{q}}^{\mu}/|\tilde{u}_{m\hat{q}}^{\mu}|$, where the eigenvectors $w_{m\hat{q}}^{\kappa\mu}$ and the displacement vectors $u_{m\hat{q}}^{\kappa\mu}$ are related by $u_{m\hat{q}}^{\kappa\mu} = w_{m\hat{q}}^{\kappa\mu}/\sqrt{M_{\kappa}}$.

In Table II we collect the velocities of sound for all copper oxide phases, as well as experimental data from the literature [71,128,136]. Values have been calculated with and without

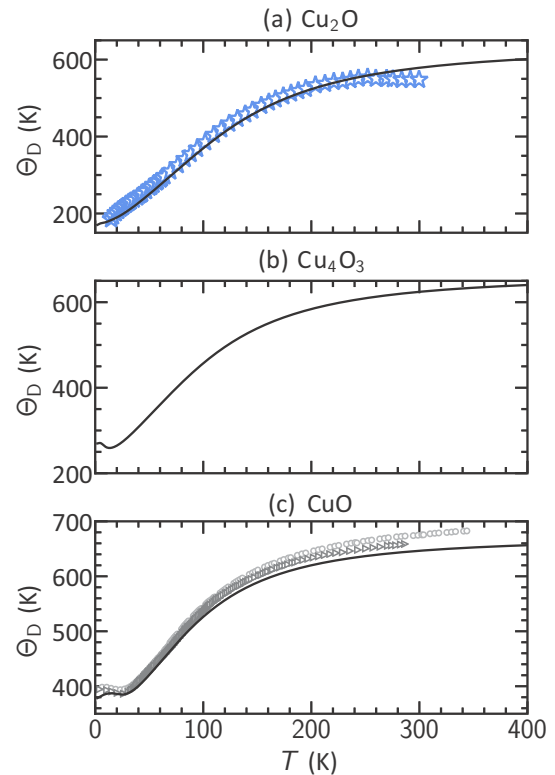


FIG. 5. Debye temperature Θ_D versus temperature T extracted from calculated (measured) heat capacities for (a) Cu_2O , (b) Cu_4O_3 , and (c) CuO . Calculated results are shown as solid black lines where Eq. (28) has been used. Experimental values in (a) for Cu_2O are taken from Ref. [127] (blue stars). In (c) for CuO experimental data from Loram *et al.* [132] (light-gray circles), and Gmelin *et al.* [134] (dark-gray triangles) is shown.

TABLE II. Velocities of sound $v_{m,\hat{\mathbf{q}}}^{\text{sound}}$ along direction $\hat{\mathbf{q}}$ of phonon modes with mainly longitudinal (l) or transversal (t) polarization (m). Velocities are listed with [Eq. (24)] and without dipole-dipole corrections. For reference, values for the derivative of the phonon dispersion from finite differences (step width $\Delta q = 10^{-4}$ bohr $^{-1}$) are given in braces. Where available, experimental data are shown for comparison. For monoclinic CuO the directions are labeled as in Ref. [71]. For Cu₄O₃ the directions refer to a body-centered tetragonal lattice [137], not to the conventional choice of the unit cell. The estimated accuracy for the velocities is $\sim 10^{-2}$ km s $^{-1}$. More digits, however, are given to capture the differences between values from numerical differentiation and values from the perturbationlike treatment.

Phase	$\hat{\mathbf{q}}$	m	$v_{m,\hat{\mathbf{q}}}^{\text{sound}}$ (km s $^{-1}$)		Experiment
			Dipole-dipole corrections (this work):		
			with	without	
Cu ₂ O	[100]	l	4.571 (4.571)	4.687 (4.687)	4.48 ^a , 4.49 ^b
		t	1.150 (1.150), 1.150 (1.150)	1.150 (1.150), 1.150 (1.150)	1.41 ^a , 1.42 ^b
	[110]	l	4.554 (4.554)	4.527 (4.527)	4.55 ^a , 4.55 ^b
		t	1.150 (1.150), 1.216 (1.216)	1.150 (1.150), 1.671 (1.671)	1.14 ^a , 1.14 ^b , 1.41 ^b
	[111]	l	4.549 (4.549)	4.473 (4.473)	–
		t	1.194 (1.194), 1.194 (1.194)	1.517 (1.517), 1.517 (1.517)	–
CuO	[100]	l	5.979 (5.979)	5.647 (5.647)	6.4 ^c
		t	2.427 (2.428), 3.834 (3.834)	1.549 (1.551), 3.900 (3.900)	–
	[010]	l	3.941 (3.942)	4.518 (4.519)	4.1 ^c
		t	1.760 (1.761), 3.863 (3.863)	1.759 (1.760), 3.859 (3.860)	–
	[001]	l	7.070 (7.071)	7.360 (7.360)	7.8 ^c
		t	1.971 (1.972), 2.366 (2.367)	2.082 (2.083), 3.199 (3.199)	–
	[101]	l	4.830 (4.831)	4.830 (4.831)	5.4 ^c
		t	2.748 (2.749), 3.685 (3.685)	2.873 (2.874), 3.685 (3.685)	–
	[10 $\bar{1}$]	l	7.012 (7.012)	7.012 (7.012)	9.1 ^c
		t	3.590 (3.591), 3.777 (3.778)	3.614 (3.615), 3.777 (3.778)	–
	[11 $\bar{1}$]	l	6.205 (6.205)	6.182 (6.182)	6.8 ^c
		t	1.605 (1.606), 3.466 (3.466)	2.338 (2.339), 3.481 (3.482)	–
Cu ₄ O ₃	[010]	l	5.328 (5.328)	5.372 (5.372)	–
		t	1.225 (1.226), 2.794 (2.794)	1.254 (1.255), 2.891 (2.891)	–
	[11 $\bar{1}$]	l	6.420 (6.420)	6.538 (6.538)	–
		t	1.575 (1.576), 1.575 (1.576)	1.988 (1.989), 1.988 (1.989)	–
	[001]	l	4.538 (4.538)	4.531 (4.531)	–
		t	1.540 (1.541), 3.435 (3.435)	1.377 (1.378), 3.503 (3.503)	–
	[111]	l	4.637 (4.638)	4.620 (4.620)	–
		t	2.125 (2.126), 3.229 (3.229)	2.159 (2.159), 3.323 (3.323)	–

^aReference [136].

^bReference [128].

^cReference [71].

dipole-dipole corrections. The derivatives have been obtained with the perturbative treatment [Eq. (24)] and by numerical differentiation (finite differences) of the phonon dispersion. The nice agreement between results obtained from both methods validates the technically quite involved perturbative approach.

Indeed, if velocities of sound are required for a few directions only, they can also be calculated from finite differences of the acoustic branches instead of using the perturbative treatment yielding Eq. (24). Of course, both methods can be expected to deliver comparable results. However, if for example lattice thermal conductivities are desired (see, e.g., Togo *et al.* [114]), phonon group velocities must be summed over the entire BZ. This clearly requires an automatization of the process of calculating the derivatives of the phonon dispersion and therefore a perturbative approach, which does not rely on additional numerical parameters, i.e., a numerical step width for the differentiation. Our method can be generalized to finite \mathbf{q} vectors and therefore has a much wider range of applicability than a finite difference calculation.

Agreement with experiment is reasonably good for Cu₂O and CuO, only for the [001], [101], and the [10 $\bar{1}$] direction in case of CuO the computed longitudinal velocity of sound is vastly too small. We have, however, to bear in mind that the results in Ref. [71] have been determined at room temperature (296 K), whereas we have considered the AFM ground state [32].

While for many directions values for the velocities of sound obtained with/without dipole-dipole corrections are close, the dipole-dipole corrections can have non-negligible influence (see, e.g., the smallest transversal velocities along the [100],[11 $\bar{1}$] directions for CuO, and along the [11 $\bar{1}$] direction for Cu₄O₃) for certain directions. Differences between the averaged velocities of sound ($v_{\text{av}}^{\text{sound}} = \frac{1}{3} \sum_{m=1}^3 \frac{1}{4\pi} \int d\hat{\mathbf{q}} v_{m\hat{\mathbf{q}}}^{\text{sound}}$) calculated without/with dipole-dipole corrections are $\sim 5\%$ for Cu₂O, $\sim 2\%$ for Cu₄O₃, and $\sim 3\%$ for CuO.

Dipole-dipole corrections can alter the slope of the acoustic branches for small values of $|\mathbf{q}|$ because such long-wavelength vibrations couple atoms at large distances $|\mathbf{d}_{\nu'\kappa'}^{0\kappa}|$, thereby

depending on long-ranged FCs. Since the method of Gonze and Lee [92] is meant to correct the long-ranged interactions, differences in the acoustic branches (at least for certain directions $\hat{\mathbf{q}}$) appear plausible. Indeed, as discussed by Gaál-Nagy [138], an insufficient description of the long-ranged interactions can lead to artificial imaginary modes (also for nonpolar semiconductors), if the grid of wave vectors on which full dynamical matrices initially are obtained (i.e., the grids $\mathcal{G}, \mathcal{G}_c$ from Secs. II A and II B) is not dense enough around $\mathbf{q} = \mathbf{0}$. During our investigations, we have found cases in which Fourier interpolation based on Eq. (2) led to imaginary modes for acoustic branches. Usage of dipole-dipole corrections [with Eq. (3)] then erased the imaginary modes leading to a much more reasonable description.

IV. CONCLUSION

In conclusion, we have discussed vibrational properties of the three copper oxide phases Cu_2O , Cu_4O_3 , and CuO , where the correct AFM ground state [32] has been considered for the latter phase. Good agreement with experiment has

been found, particularly for the vibrational heat capacity at constant volume and the vibrational entropy. Furthermore, we addressed the problem of including dipole-dipole corrections from the method due to Gonze and Lee [92] into the full dynamical matrices from the direct method. The influence on the phonon dispersion relation has been thoroughly assessed for all phases. Based on this method, we developed a scheme that allows the calculation of first-order derivatives of the phonon mode frequencies with respect to the wave vector which can be particularly useful for calculating acoustic phonon sound velocities.

ACKNOWLEDGMENTS

The authors feel obliged to the late Bruno K. Meyer for his persistent support and for numerous enlightening discussions. Computational resources have partly been provided by the Center for Scientific Computing (LOEWE-CSC) of the Goethe University Frankfurt. M.H. and C.H. acknowledge financial support within the LOEWE program of excellence of the Federal State of Hessen (project initiative STORE-E).

-
- [1] L. O. Grondahl, *Rev. Mod. Phys.* **5**, 141 (1933).
 - [2] W. H. Brattain, *Rev. Mod. Phys.* **23**, 203 (1951).
 - [3] Y. Wang, P. Miska, D. Pilloud, D. Horwat, F. Mücklich, and J. F. Pierson, *J. Appl. Phys.* **115**, 073505 (2014).
 - [4] P. W. Baumeister, *Phys. Rev.* **121**, 359 (1961).
 - [5] S. P. Tandon and J. P. Gupta, *Phys. Status Solidi B* **37**, 43 (1970).
 - [6] B. Rai, *Solar Cells* **25**, 265 (1988).
 - [7] J. Ghijsen, L. H. Tjeng, J. van Elp, H. Eskes, J. Westerink, G. A. Sawatzky, and M. T. Czyzyk, *Phys. Rev. B* **38**, 11322 (1988).
 - [8] A. Önsten, M. Månsson, T. Claesson, T. Muro, T. Matsushita, T. Nakamura, T. Kinoshita, U. O. Karlsson, and O. Tjernberg, *Phys. Rev. B* **76**, 115127 (2007).
 - [9] J. P. Hu, D. J. Payne, R. G. Egdell, P.-A. Glans, T. Learmonth, K. E. Smith, J. Guo, and N. M. Harrison, *Phys. Rev. B* **77**, 155115 (2008).
 - [10] B. K. Meyer, A. Polity, D. Reppin, M. Becker, P. Hering, P. J. Klar, T. Sander, C. Reindl, J. Benz, M. Eickhoff, C. Heiliger, M. Heinemann, J. Bläsing, A. Krost, S. Shokovets, C. Müller, and C. Ronning, *Phys. Status Solidi B* **249**, 1487 (2012).
 - [11] T. Minami, Y. Nishi, and T. Miyata, *Appl. Phys. Lett.* **105**, 212104 (2014).
 - [12] Y. Ievskaya, R. Hoye, A. Sadhanala, K. Musselman, and J. MacManus-Driscoll, *Solar Energy Mater. Solar Cells* **135**, 43 (2015).
 - [13] Y. Wang, S. Lany, J. Ghanbaja, Y. Fagot-Revurat, Y. P. Chen, F. Soldera, D. Horwat, F. Mücklich, and J. F. Pierson, *Phys. Rev. B* **94**, 245418 (2016).
 - [14] J. Dahl and A. Switendick, *J. Phys. Chem. Solids* **27**, 931 (1966).
 - [15] P. Marksteiner, P. Blaha, and K. Schwarz, *Z. Phys. B: Condens. Matter* **64**, 119 (1986).
 - [16] W. Y. Ching, Y.-N. Xu, and K. W. Wong, *Phys. Rev. B* **40**, 7684 (1989).
 - [17] E. Ruiz, S. Alvarez, P. Alemany, and R. A. Evarestov, *Phys. Rev. B* **56**, 7189 (1997).
 - [18] R. Laskowski, P. Blaha, and K. Schwarz, *Phys. Rev. B* **67**, 075102 (2003).
 - [19] X.-G. Yan, L. Xu, W.-Q. Huang, G.-F. Huang, Z.-M. Yang, S.-Q. Zhan, and J.-P. Long, *Mater. Sci. Semicond. Process.* **23**, 34 (2014).
 - [20] M. Nolan and S. D. Elliott, *Phys. Chem. Chem. Phys.* **8**, 5350 (2006).
 - [21] F. Bruneval, N. Vast, L. Reining, M. Izquierdo, F. Sirotti, and N. Barrett, *Phys. Rev. Lett.* **97**, 267601 (2006).
 - [22] T. Kotani, M. van Schilfgaarde, and S. V. Faleev, *Phys. Rev. B* **76**, 165106 (2007).
 - [23] D. O. Scanlon, B. J. Morgan, and G. W. Watson, *J. Chem. Phys.* **131**, 124703 (2009).
 - [24] D. O. Scanlon, B. J. Morgan, G. W. Watson, and A. Walsh, *Phys. Rev. Lett.* **103**, 096405 (2009).
 - [25] F. Tran and P. Blaha, *Phys. Rev. B* **83**, 235118 (2011).
 - [26] M. Heinemann, B. Eifert, and C. Heiliger, *Phys. Rev. B* **87**, 115111 (2013).
 - [27] X. G. Zheng, C. N. Xu, Y. Tomokiyo, E. Tanaka, H. Yamada, and Y. Soejima, *Phys. Rev. Lett.* **85**, 5170 (2000).
 - [28] C. E. Ekuma, V. I. Anisimov, J. Moreno, and M. Jarrell, *Eur. Phys. J. B* **87**, 23 (2014).
 - [29] X. Rocquefelte, M.-H. Whangbo, A. Villesuzanne, S. Jobic, F. Tran, K. Schwarz, and P. Blaha, *J. Phys.: Condens. Matter* **22**, 045502 (2010).
 - [30] C. Rödl, F. Sottile, and L. Reining, *Phys. Rev. B* **91**, 045102 (2015).
 - [31] S. Åsbrink and L.-J. Norrby, *Acta Crystallogr. Sect. B* **26**, 8 (1970).
 - [32] J. B. Forsyth, P. J. Brown, and B. M. Wanklyn, *J. Phys. C: Solid State Phys.* **21**, 2917 (1988).
 - [33] B. X. Yang, J. M. Tranquada, and G. Shirane, *Phys. Rev. B* **38**, 174 (1988).

- [34] B. X. Yang, T. R. Thurston, J. M. Tranquada, and G. Shirane, *Phys. Rev. B* **39**, 4343 (1989).
- [35] M. Aïn, W. Reichardt, B. Hennion, G. Pepy, and B. M. Wanklyn, *Physica C: Supercond.* **162**, 1279 (1989).
- [36] P. J. Brown, T. Chattopadhyay, J. B. Forsyth, and V. Nunez, *J. Phys.: Condens. Matter* **3**, 4281 (1991).
- [37] H. Yamada, X.-G. Zheng, Y. Soejima, and M. Kawaminami, *Phys. Rev. B* **69**, 104104 (2004).
- [38] K.-Y. Choi, W.-J. Lee, A. Glamazda, P. Lemmens, D. Wulferding, Y. Sekio, and T. Kimura, *Phys. Rev. B* **87**, 184407 (2013).
- [39] M.-H. Whangbo and H.-J. Koo, *Inorg. Chem.* **41**, 3570 (2002).
- [40] J. Pierson, A. Thobor-Keck, and A. Billard, *Appl. Surf. Sci.* **210**, 359 (2003).
- [41] J. Pierson, E. Duverger, and O. Banakh, *J. Solid State Chem.* **180**, 968 (2007).
- [42] L. Debbichi, M. C. M. de Lucas, and P. Krüger, *Mater. Chem. Phys.* **148**, 293 (2014).
- [43] M. O’Keeffe, *J. Chem. Phys.* **39**, 1789 (1963).
- [44] K. Huang, *Z. Phys.* **171**, 213 (1963).
- [45] E. C. Heltemes, *Phys. Rev.* **141**, 803 (1966).
- [46] M. Balkanski, M. A. Nusimovici, and J. Reydellet, *Solid State Commun.* **7**, 815 (1969).
- [47] C. Carabatos, *Phys. Status Solidi B* **37**, 773 (1970).
- [48] C. Carabatos and B. Prevot, *Phys. Status Solidi B* **44**, 701 (1971).
- [49] J. Reydellet, M. Balkanski, and D. Trivich, *Phys. Status Solidi B* **52**, 175 (1972).
- [50] P. F. Williams and S. P. S. Porto, *Phys. Rev. B* **8**, 1782 (1973).
- [51] P. Dawson, M. M. Hargreave, and G. Wilkinson, *J. Phys. Chem. Solids* **34**, 2201 (1973).
- [52] A. Compaan and H. Z. Cummins, *Phys. Rev. Lett.* **31**, 41 (1973).
- [53] P. Y. Yu, Y. R. Shen, Y. Petroff, and L. M. Falicov, *Phys. Rev. Lett.* **30**, 283 (1973).
- [54] P. Yu, Y. Shen, and Y. Petroff, *Solid State Commun.* **12**, 973 (1973).
- [55] C.-H. Wu and J. L. Birman, *Solid State Commun.* **14**, 465 (1974).
- [56] P. Y. Yu and Y. R. Shen, *Phys. Rev. Lett.* **32**, 373 (1974).
- [57] A. Compaan, *Solid State Commun.* **16**, 293 (1975).
- [58] Y. Petroff, P. Y. Yu, and Y. R. Shen, *Phys. Rev. B* **12**, 2488 (1975).
- [59] D. Powell, A. Compaan, J. R. Macdonald, and R. A. Forman, *Phys. Rev. B* **12**, 20 (1975).
- [60] M. M. Beg and S. M. Shapiro, *Phys. Rev. B* **13**, 1728 (1976).
- [61] P. Y. Yu and Y. R. Shen, *Phys. Rev. B* **17**, 4017 (1978).
- [62] M. A. Washington, A. Z. Genack, H. Z. Cummins, R. H. Bruce, A. Compaan, and R. A. Forman, *Phys. Rev. B* **15**, 2145 (1977).
- [63] K. Reimann and K. Syassen, *Phys. Rev. B* **39**, 11113 (1989).
- [64] M. Ivanda, D. Waasmaier, A. Endriss, J. Ihringer, A. Kirfel, and W. Kiefer, *J. Raman Spectrosc.* **28**, 487 (1997).
- [65] R. Mittal, S. L. Chaplot, S. K. Mishra, and P. P. Bose, *Phys. Rev. B* **75**, 174303 (2007).
- [66] K.-P. Bohnen, R. Heid, L. Pintschovius, A. Soon, and C. Stämpfl, *Phys. Rev. B* **80**, 134304 (2009).
- [67] T. Sander, C. T. Reindl, M. Giar, B. Eifert, M. Heinemann, C. Heiliger, and P. J. Klar, *Phys. Rev. B* **90**, 045203 (2014).
- [68] Z. Popovic, C. Thomsen, M. Cardona, R. Liu, G. Stanisic, R. Kremer, and W. König, *Solid State Commun.* **66**, 965 (1988).
- [69] J. Chrzanowski and J. C. Irwin, *Solid State Commun.* **70**, 11 (1989).
- [70] A. Junod, D. Eckert, G. Triscone, J. Müller, and W. Reichardt, *J. Phys.: Condens. Matter* **1**, 8021 (1989).
- [71] W. Reichardt, F. Gompf, M. Aïn, and B. M. Wanklyn, *Z. Phys. B: Condens. Matter* **81**, 19 (1990).
- [72] H. Hagemann, H. Bill, W. Sadowski, E. Walker, and M. François, *Solid State Commun.* **73**, 447 (1990).
- [73] H. F. Goldstein, D. S. Kim, P. Y. Yu, L. C. Bourne, J.-P. Chaminade, and L. Nganga, *Phys. Rev. B* **41**, 7192 (1990).
- [74] J. Irwin, J. Chrzanowski, T. Wei, D. Lockwood, and A. Wold, *Physica C: Supercond.* **166**, 456 (1990).
- [75] K. Reimann and K. Syassen, *Solid State Commun.* **76**, 137 (1990).
- [76] G. Kliche and Z. V. Popovic, *Phys. Rev. B* **42**, 10060 (1990).
- [77] J. C. Irwin, T. Weit, and J. Franck, *J. Phys.: Condens. Matter* **3**, 299 (1991).
- [78] S. Guha, D. Peebles, and T. J. Wieting, *Bull. Mater. Sci.* **14**, 539 (1991).
- [79] S. Guha, D. Peebles, and T. J. Wieting, *Phys. Rev. B* **43**, 13092 (1991).
- [80] S. Narang, V. Kartha, and N. Patel, *Physica C: Supercond.* **204**, 8 (1992).
- [81] C. C. Homes, M. Ziaei, B. P. Clayman, J. C. Irwin, and J. P. Franck, *Phys. Rev. B* **51**, 3140 (1995).
- [82] X. K. Chen, J. C. Irwin, and J. P. Franck, *Phys. Rev. B* **52**, R13130(R) (1995).
- [83] A. B. Kuz’menko, D. van der Marel, P. J. M. van Bentum, E. A. Tishchenko, C. Presura, and A. A. Bush, *Phys. Rev. B* **63**, 094303 (2001).
- [84] Z. Wang, V. Pischedda, S. K. Saxena, and P. Lazor, *Solid State Commun.* **121**, 275 (2002).
- [85] L. Debbichi, M. C. M. de Lucas, J. F. Pierson, and P. Krüger, *J. Phys. Chem. C* **116**, 10232 (2012).
- [86] A. P. Litvinchuk, A. Möller, L. D. P. Krüger, M. N. Iliev, and M. M. Gospodinov, *J. Phys.: Condens. Matter* **25**, 105402 (2013).
- [87] G. Kresse, J. Furthmüller, and J. Hafner, *Europhys. Lett.* **32**, 729 (1995).
- [88] K. Parlinski, Z.-Q. Li, and Y. Kawazoe, *Phys. Rev. Lett.* **78**, 4063 (1997).
- [89] A. van de Walle and G. Ceder, *Rev. Mod. Phys.* **74**, 11 (2002).
- [90] P. Giannozzi, S. de Gironcoli, P. Pavone, and S. Baroni, *Phys. Rev. B* **43**, 7231 (1991).
- [91] X. Gonze, *Phys. Rev. B* **55**, 10337 (1997).
- [92] X. Gonze and C. Lee, *Phys. Rev. B* **55**, 10355 (1997).
- [93] S. Baroni, S. de Gironcoli, A. Dal Corso, and P. Giannozzi, *Rev. Mod. Phys.* **73**, 515 (2001).
- [94] M. K. Gupta, R. Mittal, S. L. Chaplot, and S. Rols, *J. Appl. Phys.* **115**, 093507 (2014).
- [95] L. H. N. Rimmer, M. T. Dove, B. Winkler, D. J. Wilson, K. Refson, and A. L. Goodwin, *Phys. Rev. B* **89**, 214115 (2014).
- [96] A. A. Maradudin, E. W. Montroll, G. H. Weiss, and I. P. Ipatova, *Theory of Lattice Dynamics in the Harmonic Approximation*, 2nd ed., edited by H. Ehrenreich, F. Seitz, and D. Turnbull, Suppl. 3 (Academic, New York, 1971).
- [97] X. Gonze, B. Amadon, P.-M. Anglade, J.-M. Beuken, F. Bottin, P. Boulanger, F. Bruneval, D. Caliste, R. Caracas, M. Côté, T. Deutsch, L. Genovese, P. Ghosez, M. Giantomassi, S. Goedecker, D. Hamann, P. Hermet, F. Jollet, G. Jomard, S. Leroux, M. Mancini, S. Mazevet, M. Oliveira, G. Onida,

- Y. Pouillon, T. Rangel, G.-M. Rignanese, D. Sangalli, R. Shaltaf, M. Torrent, M. Verstraete, G. Zérah, and J. Zwanziger, *Comput. Phys. Commun.* **180**, 2582 (2009).
- [98] P. Giannozzi, S. Baroni, N. Bonini, M. Calandra, R. Car, C. Cavazzoni, D. Ceresoli, G. L. Chiarotti, M. Cococcioni, I. Dabo, A. D. Corso, S. de Gironcoli, S. Fabris, G. Fratesi, R. Gebauer, U. Gerstmann, C. Gougoussis, A. Kokalj, M. Lazzeri, L. Martin-Samos, N. Marzari, F. Mauri, R. Mazzarello, S. Paolini, A. Pasquarello, L. Paulatto, C. Sbraccia, S. Scandolo, G. Sclauzero, A. P. Seitsonen, A. Smogunov, P. Umari, and R. M. Wentzcovitch, *J. Phys.: Condens. Matter* **21**, 395502 (2009).
- [99] M. Born and K. Huang, *Dynamical Theory of Crystal Lattices*, edited by E. F. Mott, E. C. Bullard, and D. H. Wilkinson (Oxford University Press, Oxford, 1954).
- [100] G. Kresse and J. Hafner, *Phys. Rev. B* **47**, 558 (1993).
- [101] G. Kresse and J. Hafner, *Phys. Rev. B* **49**, 14251 (1994).
- [102] G. Kresse and J. Furthmüller, *Comput. Mater. Sci.* **6**, 15 (1996).
- [103] G. Kresse and J. Furthmüller, *Phys. Rev. B* **54**, 11169 (1996).
- [104] G. Kern, G. Kresse, and J. Hafner, *Phys. Rev. B* **59**, 8551 (1999).
- [105] Y. Wang, J. J. Wang, W. Y. Wang, Z. G. Mei, S. L. Shang, L. Q. Chen, and Z. K. Liu, *J. Phys.: Condens. Matter* **22**, 202201 (2010).
- [106] Y. Wang, L. A. Zhang, S. Shang, Z.-K. Liu, and L.-Q. Chen, *Phys. Rev. B* **88**, 024304 (2013).
- [107] Y. Wang, J. E. Saal, Z. Mei, P. Wu, J. Wang, S. Shang, Z.-K. Liu, and L.-Q. Chen, *Appl. Phys. Lett.* **97**, 162907 (2010).
- [108] Y. Wang, J. E. Saal, J.-J. Wang, A. Saengdeejing, S.-L. Shang, L.-Q. Chen, and Z.-K. Liu, *Phys. Rev. B* **82**, 081104 (2010).
- [109] Y. Wang, J. J. Wang, J. E. Saal, S. L. Shang, L.-Q. Chen, and Z.-K. Liu, *Phys. Rev. B* **82**, 172503 (2010).
- [110] Y. Wang, J. E. Saal, P. Wu, J. Wang, S. Shang, Z.-K. Liu, and L.-Q. Chen, *Acta Mater.* **59**, 4229 (2011).
- [111] Y. Wang, H. Fang, C. L. Zacherl, Z. Mei, S. Shang, L.-Q. Chen, P. D. Jablonski, and Z.-K. Liu, *Surf. Sci.* **606**, 1422 (2012).
- [112] Y. Wang, S. Shang, Z.-K. Liu, and L.-Q. Chen, *Phys. Rev. B* **85**, 224303 (2012).
- [113] Y. Wang, L.-Q. Chen, and Z.-K. Liu, *Comput. Phys. Commun.* **185**, 2950 (2014).
- [114] A. Togo, L. Chaput, and I. Tanaka, *Phys. Rev. B* **91**, 094306 (2015).
- [115] A. Togo, F. Oba, and I. Tanaka, *Phys. Rev. B* **78**, 134106 (2008).
- [116] R. Dovesi, R. Orlando, A. Erba, C. M. Zicovich-Wilson, B. Civalieri, S. Casassa, L. Maschio, M. Ferrabone, M. De La Pierre, P. D'Arco, Y. Noël, M. Causà, M. Rérat, and B. Kirtman, *Int. J. Quantum Chem.* **114**, 1287 (2014).
- [117] W. Li, J. Carrete, N. A. Katcho, and N. Mingo, *Comput. Phys. Commun.* **185**, 1747 (2014).
- [118] A. Chernatynskiy and S. R. Phillpot, *Comput. Phys. Commun.* **192**, 196 (2015).
- [119] Y. Wang, S.-L. Shang, H. Fang, Z.-K. Liu, and L.-Q. Chen, *Npj Comput. Mater.* **2**, 16006 (2016).
- [120] P. E. Blöchl, *Phys. Rev. B* **50**, 17953 (1994).
- [121] G. Kresse and D. Joubert, *Phys. Rev. B* **59**, 1758 (1999).
- [122] A. I. Liechtenstein, V. I. Anisimov, and J. Zaanen, *Phys. Rev. B* **52**, R5467(R) (1995).
- [123] V. I. Anisimov, J. Zaanen, and O. K. Andersen, *Phys. Rev. B* **44**, 943 (1991).
- [124] M. O'Keeffe and J.-O. Bovin, *Am. Mineral.* **63**, 180 (1978).
- [125] J. H. Lloyd-Williams and B. Monserrat, *Phys. Rev. B* **92**, 184301 (2015).
- [126] G. E. Kugel, C. Carabatos, and W. Kress, *Ab Initio Calculation of Phonon Spectra* (Plenum, New York, 1983), p. 101.
- [127] J.-H. Hu and H. L. Johnston, *J. Am. Chem. Soc.* **73**, 4550 (1951).
- [128] M. H. Manghnani, W. S. Brower, and H. S. Parker, *Phys. Status Solidi A* **25**, 69 (1974).
- [129] O. Madelung, U. Rössler, and M. Schulz (eds.), *Landolt-Börnstein: Numerical Data and Functional Relationships in Science and Technology*, C: Non-Tetrahedrally Bonded Elements and Binary Compounds I, Vol. III/41 (Springer, Berlin, 1998).
- [130] G. K. White, *J. Phys. C: Solid State Phys.* **11**, 2171 (1978).
- [131] J.-H. Hu and H. L. Johnston, *J. Am. Chem. Soc.* **75**, 2471 (1953).
- [132] J. W. Loram, K. A. Mirza, C. P. Joyce, and A. J. Osborne, *Europhys. Lett.* **8**, 263 (1989).
- [133] R. W. Millar, *J. Am. Chem. Soc.* **51**, 215 (1929).
- [134] E. Gmelin, W. Brill, and T. Chattopadhyay, *Thermochim. Acta* **160**, 43 (1990).
- [135] E. Gmelin, U. Köbler, W. Brill, T. Chattopadhyay, and S. Sastry, *Bull. Mater. Sci.* **14**, 117 (1991).
- [136] J. Berger, *Solid State Commun.* **26**, 403 (1978).
- [137] C. J. Bradley and A. P. Cracknell, *The Mathematical Theory of Symmetry in Solids* (Oxford University Press, Oxford, 1972).
- [138] K. Gaál-Nagy, *Phys. Rev. B* **77**, 024309 (2008).